Spin probe reorientation and its dynamic heterogeneity in relation to free volume and relaxation dynamics in oligomer *cis-1,4-poly(isoprene)*

H.Švajdlenková,[1] S.Arrese-Igor,[2,3] Z.Nógellová,[1] A.Alegría,[2,3] and J.Bartoš[1*]

[1] Department of Structure and physical properties, Polymer Institute of SAS, Dúbravská cesta 9, SK-845 41 Bratislava, Slovakia

[2] Centro de Fisica de Materiales, CSIC - UPV/EHU, P[0] M.de Lardizabal 5, 20018 San Sebastián, Spain

[3] Departamento de Fisica de Materiales, UPV/EHU, Apdo 1072, 20080 San Sebastián, Spain

Abstract

A combined study of the molecular *guest* rotation dynamics and the *host* free volume in oligomeric **cis -1,4–poly (isoprene) (cis-1,4-PIP)** by means of two external probings using **electron spin resonance (ESR)** and **positron annihilation lifetime spectroscopy (PALS)** together with electric dipole relaxation dynamics via **broadband dielectric spectroscopy** (**BDS**) is presented. The spectral evolution of **2,2,6,6-tetramethylpiperidinyl-1-oxy** (**TEMPO**) from spectral simulations over a wide range from 100 K up to 300 K reveals three different regions of mobility consisting of a slow regime at low T's followed by the dynamic heterogeneity zone at intermediate T's from 155 K < T_g^{DSC} up to 235 K > T_g^{DSC} and ending with a fast regime at high T 's with the characteristic **ESR** temperatures: $T_{X1}^{s} = T_{X1}^{f}$ = 155 K, T_{X2}^{s} = 186 K, T_c = 235 K and T_{X1}^{f} = 263 K. These are in close coincidence with four characteristic **PALS** temperatures: T_{b1}^{G} = 160 K, T_g^{PALS} = 190 K, T_{b1}^{L} = 227 K and T_{b2}^{L} = 263 K. Finally, by internal dynamic probing via **BDS** we reveal that the various aspects of the structural relaxation of **1,4-PIP 0.8k** are responsible for the *liquid* state effects in the **ESR** and **PALS** response, i.e., the onset of the segmental α process for $T_c \cong T_{b1}^{L}$ and the maximum of the segmental α process for $T_{X1}^{f} \cong T_{b2}^{L}$.

Keywords: *guest* dynamics, dynamic heterogeneity, **ESR**, *host* free volume, **PALS**, *host* relaxation dynamics, **BDS**

1. Introduction

One of the persisting and still unresolved tasks in the condensed and soft matter physics is to reveal the physical mechanism which governs the structural and dynamics evolution of all the types glass-formers on their way from the stable normal liquid state via the meta-stable supercooled liquid one followed by liquid to glass transition down to the glassy solid state on decreasing temperature [1,2]. Traditionally, a direct approach to the structural and dynamic characterization of glass-formers includes the *internal* probes such as static density fluctuation via **x-ray** and **neutron diffraction** or various dynamic "markers" such as dynamic density fluctuation via **neutron scattering (NS)** [3], nuclear magnetic dipoles in **nuclear magnetic resonance (NMR)** [4] and effective electric dipoles in **broadband dielectric spectroscopy**

(BDS) [5]. The most characteristic observations are significant deviations from the ideal exponential **Debye law** for the time evolution of the relaxing quantity of the observed processes and from the ideal exponential **Arrhenius law** for the temperature dependence of the time scale giving to rise non-**Debye** or non (super)-**Arrhenius** dependencies, respectively [6]. In spite of a slight change in the structural parameters, further complexity of glass-formers is that the *liquid* state over a wide temperature and time ranges include the existence of several regions of different relaxation behavior and the related crossover effects at the characteristic dynamic (DYN) temperatures [7] such as Arrhenius, T_A, Stickel, T_B^{ST}, and Schönhals, T_B^{SCH}, temperatures for the former quantity and Alegria-Colmenero one, T_B^{AC} = $T_{B^\beta KWW}$ for the latter one. Finally, the last but no longer the least aspect of the *liquid* slowing down and the glass formation is the dynamic heterogeneity of the disordered phase, i.e., different mobility of the constituents being distant a few nm away [8] considered to be responsible for the non-**Debye** type of the structural relaxation and ascribed to a distribution of relaxation times in all the three physical states [9,10].

On the other hand, glass-formers can be investigated in an indirect way utilizing *external* probes such as the **ortho-positronium** (**o-Ps**) using **positron annihilation lifetime spectroscopy (PALS)** [11] or the **stable free radicals** the so-called **spin probes** by means of **electron spin resonance** (**ESR**) [12]. Since both *external* probe techniques are sensitive to the local microstructure and the local dynamics of condensed materials, new information about various aspects of glass-formers, such a variety of crossovers in the probe dynamics, dynamic heterogeneity, etc., are expected which can be added to the *internal* probe data of the media and subsequently, to contribute to our deeper understanding of their properties.

In the former case, **o-Ps** lifetime, τ_3, as a function of temperature T reflects within the free volume concept the static and dynamic free volume [14]. This **PALS** response of a given amorphous material exhibits the monotoneous regions with a few discontinuities (bends) at several characteristic **PALS** temperatures T_{bi}^G, T_g^{PALS}, T_{b1}^L [15-18] and T_{b2}^L [15,19,20] which are sometimes compatible with the afore-mentioned characteristic DYN temperatures (T_B^{ST}, T_B^{SCH}, T_B^{AC} = $T_{B^\beta KWW}$ and T_A) as well as with the time scales of the various motional modes of the medium as obtained from **BDS**. This allows to identify the specific microscopic process responsible for the distinct bend effects at T_{b1}^L and T_{b2}^L with various aspects of primary α relaxation [21a,b,22-24] and secondary β relaxation [21b,25] from **BDS.** Two empirical regularities were revealed indicating a significant role of the former process in **o-Ps**

annihilation event, namely, i) comparability of the *mean* **PALS** and *mean* **BDS** time scales at the so-called plateau temperature T_{b2}^{L} on a few nanoseconds level: $\tau_3(T_{b2}^{L}) \cong \tau_\alpha$ [21] and ii) typical time scale at T_{b1}^{L} about a microsecond level: $\tau_\alpha(T_{b1}^{L}) = 10^{-6\pm1}$ s [22]. In addition to the *mea+n* τ_3 value representation, analyses of the PALS data by special **LT** or **MELT** programs allow to address the **o-Ps** lifetime and the related free volume size distribution aspects of the glass-forming material - see e.g. Refs.11a,b.

As for the **ESR** technique, a spectral evolution of the triplet signal from one of the smallest molecular stable radical of nitroxyl type, the so-called spin probe **2,2,6,6-tetramethyl-piperidinyl-1-oxy (TEMPO)** which reflects its rotational dynamics in a given glass-former can be utilized. The ESR response of a spin system, i.e., the temperature dependence of the spectral parameter of spin probe **TEMPO** mobility, $2A_{zz}'$, in a given **medium** can be described by several characteristic ESR temperatures, such as the most pronounced one, T_{50G}, which quantifies operationally a main transition from its slow to fast motional regime [26] together with some other ones, such as T_{Xi}^{slow} and T_{Xi}^{fast}, where i = 1 or 2, which reflect subtle changes in the spin probe dynamics within the individual motional regimes, respectively [27]. In most amorphous organics studied so far, the main characteristic **ESR** temperatures T_{50G} and T_{Xi}^{fast} are situated above glass transition temperature with T_{50G} at (1.10 - 1.50)T_g^{DSC} [28] with one exception [30] and with T_{Xi}^{fast} at (1.30-1.67)T_g^{DSC} with the relative T_{50G}/T_g^{DSC} and T_{Xi}^{fast}/T_g^{DSC} temperatures strongly dependent on the chemical nature of glass-formers. The question about the physical or physico-chemical factors controlling the spin probe **TEMPO** dynamics in both the slow and fast regimes and the origin of the both crossover **ESR** temperatures remains still open. In order to resolve this problem on some unified basis, recent comparative **ESR** and **PALS** studies revealed two empirical rules between these characteristic **ESR** temperatures of **TEMPO** and the **o-Ps** annihilation lifetime and related free volume ones in a variety of the amorphous organics [28-31]. In particular, the averaged *mean* **o-Ps** lifetimes at the main characteristic **ESR** temperature, $\tau_3(T_{50G})$, and at the other one within the fast regime, $\tau_3(T_{Xi}^{fast})$, lie in remarkably narrow ranges of 2.17±0.15 ns [28-31] or 2.85±0.18 ns [29,30], respectively. These averaged mean characteristic τ_3 values correspond according to a standard quantum-mechanical (SQM) model of **o-Ps** annihilation in a *spherical* free volume hole approximation [14], to the averaged mean free volumes of $V_h(T_{50G})$ = 114±15 Å^3 [28-31] or $V_h(T_{Xi}^{fast})$ = 185±18 Å^3, respectively, the latter one being comparable with the van der Waals volume of the **TEMPO** molecule [29-31]. These findings mean that the afore-mentioned dynamic changes of the **TEMPO** are closely connected with the presence of a

certain local free volume which appears to be almost independent of the chemical structure and the related type and extent of vdW- or H-inter-molecular bonding [28], the topology (small or short vs. long) molecules [28-31] as well as of the physical (glass vs. liquid) state [30] of amorphous organics. Moreover, in some of them a plausible agreement between the characteristic **ESR** and **PALS** temperatures was found such as $T_{50G} \cong T_{b2}^{L}$ for **glycerol (GL)** and **propylene carbonate (Pc)** or $T_{50G} \cong T_{b1}^{L}$ for **meta-tricresyl phosphate (m-TCP)** and for some polymers [27,31].This suggests that both the change in reorientation dynamics of the molecular probe **TEMPO** and the change in **o-Ps** annihilation have the similar physical origin. As mentioned above, since in the **PALS** case the T_{b2}^{L} effect is controlled by the *mean* primary α relaxation time, it implies that also the slow to fast motion regime transition could be governed by the same relaxation. However, this structural dynamics hypothesis remains to be still tested. In other case of $T_{50G} \cong T_{b1}^{L}$, and especially, for those for which $T_{b1}^{L} < T_{50G} < T_{b2}^{L}$, and similarly, the question about whether the primary or/and secondary process is/are of relevance is still unclear and needs to be clarify and forms one issue of this paper.

The above-mentioned relationships between the **ESR** and **PALS** parameters have been found for the $2A_{zz}$, quantity. Another measure of the spin probe dynamics, i.e., correlation time of spin probe rotation, τ_c, as obtained by semi-empirical equations for both the individual motion regimes [12] or more sophistically, by spectral simulations [12a,c,32-35], ranges from 10^{-6} s in the slow region down to 10^{-11} s in the fast one with a typical value at T_{50G} reaching of a few nanoseconds can be used [12]. One of the advantages of ESR technique in the spin probe version is that it can be utilized for characterization of the various types of dynamically heterogeneous systems based on the significant difference in the spectral features of the nitroxide radicals in slow and fast motion regimes in various materials [12d,13].

In this paper we address further the mutual relationships between the **ESR** and **PALS** data at level of the respective time scales by i) focusing on an aspect of the dynamic heterogeneity of the molecular spin probe **TEMPO** mobility in one-component amorphous glass-former, namely, oligomer **cis-1,4-poly(isoprene) (cis-1,4-PIP)** by means of application of appropriate spectral simulation procedure with ii) aim to identify the particular motional mode responsible for the characteristic features (temperatures) in the respective **ESR** and **PALS** responses in the *liquid* state by using relevant **BDS** technique.

2. Experimental

2.1 Materials:

Oligomeric **cis-1,4-poly(isoprene) (cis-1,4-PIP)** from Polymer Source, Canada with 80 % of cis-isomer form and the weight averaged molecular weight $\boldsymbol{M_w}$ = 904 g/mol and the number averaged molecular weight M_n = 800 g/mol giving the polydispersity index of $\boldsymbol{M_w/M_n}$ = 1.13 was used. For the sake of simplicity the abbreviation of **1,4-PIP 0.8k** in the further text is used. As the spin probe the smallest stable radical of nitroxyl type utilized in our previous ESR studies [1-6] **2,2,6,6-tetramethyl-1-piperidinyloxy (TEMPO)** from Sigma-Aldrich, Inc. Germany was applied by its solving in the liquid **cis-1,4-PIP** at concentration of about $5x10^{-4}$ spin/mol. The liquid to glass temperature of **1,4-PIP 0.8k**, was determined to be of $\boldsymbol{T_g^{DSC}}$ = 188 K from the cooling mode measurement with rate Φ_c = - 10 K/min because of the absence of overshoot using the TA Instruments DSC-Q 2000 calibrated with indium which is observed in the heating mode with rate Φ_h = + 10 K/min.

2.2 ESR

ESR measurements of spin probed **1,4-PIP 0.8k** were performed on the X-band Bruker–ER 200 SRL operating at 9.4 GHz with a Bruker BVT 100 temperature variation controller unit. ESR spectra of the slowly cooled doped **1,4-PIP 0.8k/TEMPO** system were recorded on heating mode over a wide temperature range from 100 K up to 300 K with step of 5 K. The sample was kept at the given temperature until thermal equilibrium for 15 min before the start of three spectra accumulations. The temperature stability was ± 0.5 K. The microwave power and the amplitude of the field modulation were optimized to avoid the signal distortion. Evaluation of the ESR spectra was performed in terms of the spectral parameter of mobility, $\boldsymbol{2A_{zz'}}$, as a function of temperature with subsequent evaluation of the spectral parameter of mobility $\boldsymbol{T_{50G}}$ [26] and further characteristic ESR temperatures, $\boldsymbol{T_{Xi}^{2Azz}}$**,** in both the slow and fast motional regimes [27]. Correlation time, $\boldsymbol{\tau_c}(T)$**,** as another measure of the spin probe mobility and the corresponding characteristic **ESR** temperatures such as $\boldsymbol{T_c}$ and further ones, $\boldsymbol{T_{Xi}^{c}}$, were obtained using a Non-linear Least Squares Line (NLSL) simulation program based on the isotropic Brownian model of nitroxide spin probe reorientation. The least-squares fits of experimental spectra are calculated by Stochastic Liouville equation and utilize modified Levenberg-Marquardt minimization algorithm which allow to determine both the time scales, $\boldsymbol{\tau_c^s}(T)$ and $\boldsymbol{\tau_c^f}(T)$, and the population fractions $\boldsymbol{F_s}(T)$, $\boldsymbol{F_f}(T)$ of the spin probe **TEMPO** rotation dynamics in both the slow and fast motion regimes [33].

2.3 PALS

The experimental **PALS** set up as well as the details about both the measurements and evaluation procedures utilizing **LT 9 routine** are given in the original paper devoted to a series of **cis-1,4-PIP** systems including the **1,4-PIP 0.8k** sample [31].

2.4 BDS

Broadband dielectric spectroscopic (BDS) measurements were performed by using a high resolution Novocontrol dielectric analyser in the range 10^{-2}-10^{7} Hz and an Agilent RF impedance analyzer 4291 B operating in the range 10^{6}-10^{9} Hz. Isothermal frequency scans were carried out over the temperature interval from 150 K up to 300 K with a temperature step of 5 K. The sample was placed between two parallel plate capacitor with the Teflon spacer of thickness of 100 μm. Dielectric spectra were analyzed using the Havriliak-Negami (HN) expression [5,36]:

$$\varepsilon(\omega) = \sum \varepsilon_{\infty} + \frac{\varepsilon_s - \varepsilon_{\infty}}{\left[\left(1 + i\omega\tau_{HN}\right)^{1-\alpha_{HN}}\right]^{\beta_{HN}}}$$

where, $\varepsilon_s - \varepsilon_\infty$ is the relaxation strength, τ_{HN} is the relaxation time, α_{HN} and β_{HN} are the shape parameters of the spectral peak. In the special asymmetric broadening case, the Cole - Davidson (CD) function is used with $\alpha_{HN} = 0$ and and $\beta_{HN} \neq 0$, while in the special symmetric broadening one, the spectral peak is described by Cole - Cole (CC) function with $\alpha_{HN} \neq 0$ and and $\beta_{HN} = 0$. Then, the maximum relaxation time, τ_{max}, can be calculated using these spectral parameters according to the formula [5,37]:

$$\tau_{\max} = \tau_{HN}\left[\frac{\sin\frac{\pi(1-\alpha)\beta}{2(\beta+1)}}{\sin\frac{\pi(1-\alpha)}{2(\beta+1)}}\right]^{1/(1-\alpha)}$$

3. Results

3.1 ESR data

Fig. 1displays the ESR spectral evolution of the spin system **1,4-PIP 0.8k/TEMPO** over a wide temperature range from 100 K up to 300 K. Typical spectral change of the **TEMPO** from a broad triplet from the slow moving spin probes at the lowest temperatures up to the narrow triplet from the fast moving ones at the highest temperatures is evident. On closer inspection, the spectral evolution of the spin probes **TEMPO** in **1,4-PIP 0.8k** exhibits a complex superimposed course resulting into the bimodal spectra character in the intermediate temperature range from the co-existing slow and fast moving spin probes.

As mentioned in the Introduction, the spin probe **TEMPO** mobility in the **1,4-PIP 0.8k** medium can be quantified in two ways. **Fig. 2** displays the spectral parameter of mobility given by an outer extrema line separation of triplet signal, $\mathbf{2}\boldsymbol{A}_{\boldsymbol{zz}}$', as a function of temperature $\boldsymbol{T}$. The $\mathbf{2}\boldsymbol{A}_{\boldsymbol{zz}}$', vs. $\boldsymbol{T}$ plot exhibits a quasi-sigmoidal course changing from the high value of $\mathbf{2}\boldsymbol{A}_{\boldsymbol{zz}}$', ~ 67 G in the low temperature region down to the low one $\mathbf{2}\boldsymbol{A}_{\boldsymbol{zz}}$', ~ 33 G in the high temperature one with the following features. The five regions of distinct behavior of the $\mathbf{2}\boldsymbol{A}_{\boldsymbol{zz}}$', quantity depicted 1 - 5 described by the four characteristic **ESR** temperatures are evident.

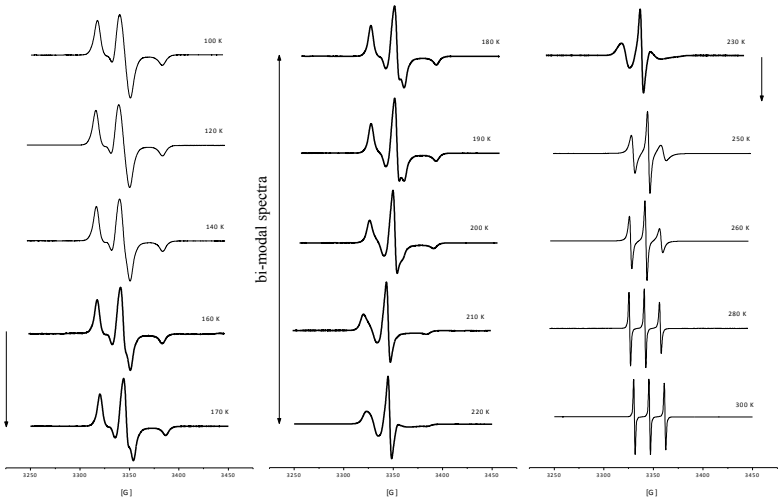

Fig.1 Spectral evolution of the spin system of **1,4-PIP 08.k/TEMPO** at selected temperature from a wide temperature interval from 100 K up to 300 K. The arrow marks region of the superimposed broad and narrow spectra.

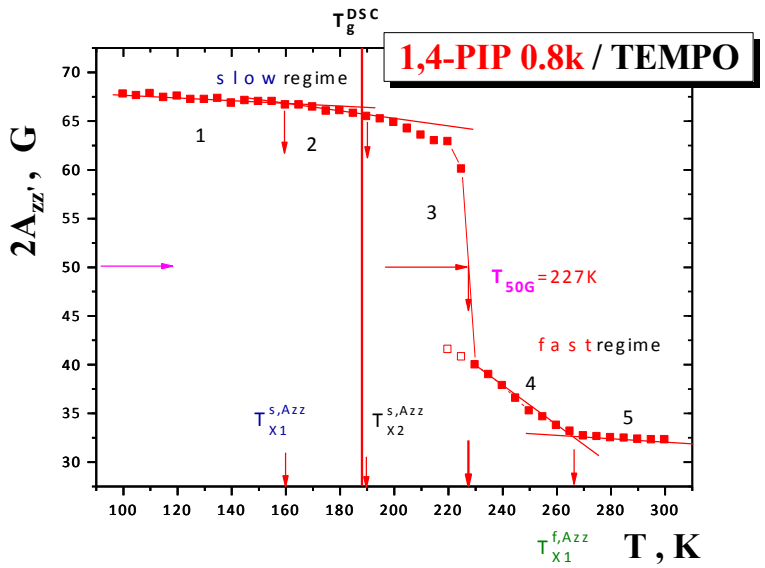

Fig.2 Spectral parameter of mobility, $2A_{zz'}$, as a function of temperature with four characteristic **ESR** temperatures $T_{X1}^{s,2Azz'}$ = 160 K, $T_{X2}^{s,2Azz'}$ = 190 K, T_{50G} = 227 K and $T_{X1}^{f,2Azz'}$ = 266 K together with T_g^{DSC} = 188 K marked by a vertical line.

The low T region of two linear regions in the slow motion regime 1 and 2 with $T_{X1}^{s,2Azz'} \cong$ 160 K and $T_{X2}^{s,2Azz} \cong$ 190 K is followed by a transition zone 3. This is operationally marked by the most pronounced characteristic **ESR** temperature, T_{50G} = 227 K. Finally, in the high T zone again two linear regions 4 and 5 define the fourth characteristic ESR temperature $T_{X1}^{f,2Azz'} \cong$ 266 K [31].

The second parameter of the spin probe dynamics, i.e., correlation time, τ_c, can be obtained using an appropriate simulation program. Here, we have used the ***NLSL*** programm based on the isotropic Brownian diffusion model of nitroxide probe reorientation [33] which is able to reproduce both the monomodal **ESR** spectra in the pure slow and pure fast regimes as well as the bimodal **ESR** spectra due to superimposition of of spin probe **TEMPO** in both the motional regimes. For the used spin probe **TEMPO** the following magnetic parameters were used for g-factor: g_{xx} = 2.0103, g_{yy} = 2.0069 and g_{zz} = 2.0030 and A-hyperfine constant tensors: A_{xx} = 7.66 G, A_{yy} = 7.1 G and A_{zz} = 16.9 G [38]. **Fig. 3** shows a comparison of the typical output of the simulation spectra with the corresponding correlation coefficient for mono- (a,c) and bimodal (b) **ESR** spectra of the spin probe **TEMPO** in **1,4-PIP 0.8k**. The bimodal superimposed ESR spectra were recognized on the basis of the quality of spectral fit reaching 0.990 – 0.999 in the temperature range from 155 K up to 230 K.

a)

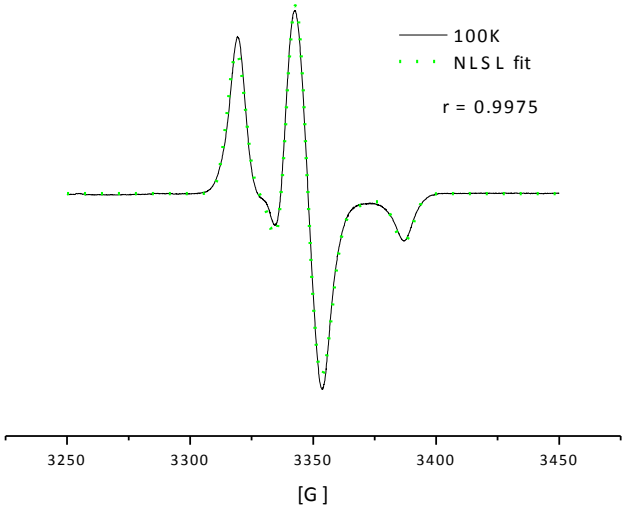
100K
NLSL fit
r = 0.9975
3250
3300
3350
3400
3450
[G]

b)

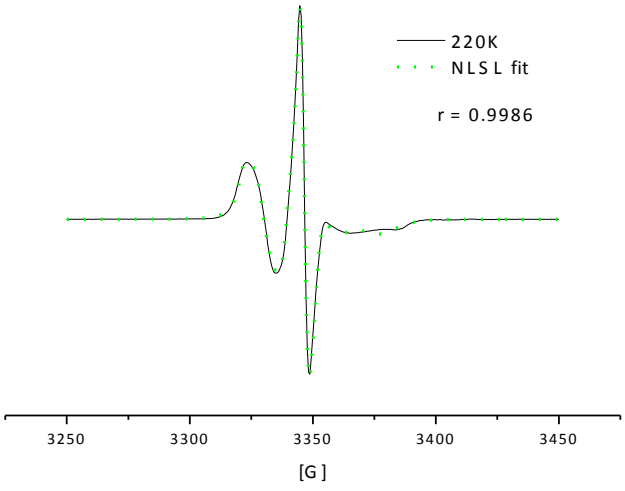
220K
NLSL fit
r = 0.9986
3250
3300
3350
3400
3450
[G]

c)

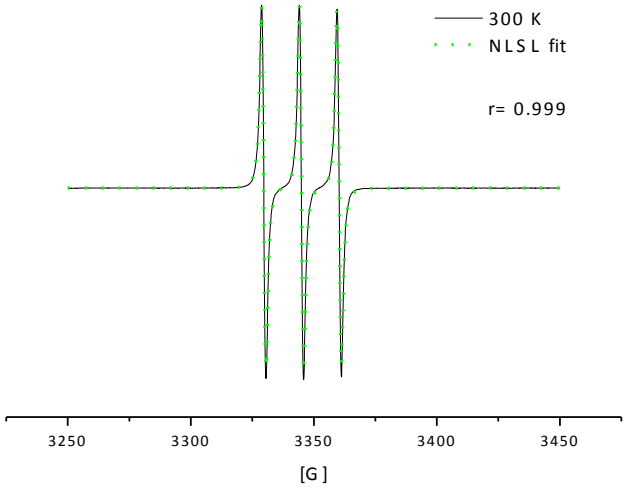

Fig. 3 Representative comparions of the experimental (black) and ***NLSL*** simulated (green) **ESR** spectra of **TEMPO** in **1,4-PIP 0.8k** in slow motion regime at 100 K (a), superimposed slow and fast motion regimes at 220 K (b) and finally, in fast motion regime (c) at 300 K together with the corresponding correlation coefficients.

Next, **Figs. 4** and **5** present the time scales, τ_c^s, τ_c^f, and the fractions, F^s, F^f, of the corresponding slow and/or fast spectral components as a function of $1/T$ or T, respectively.

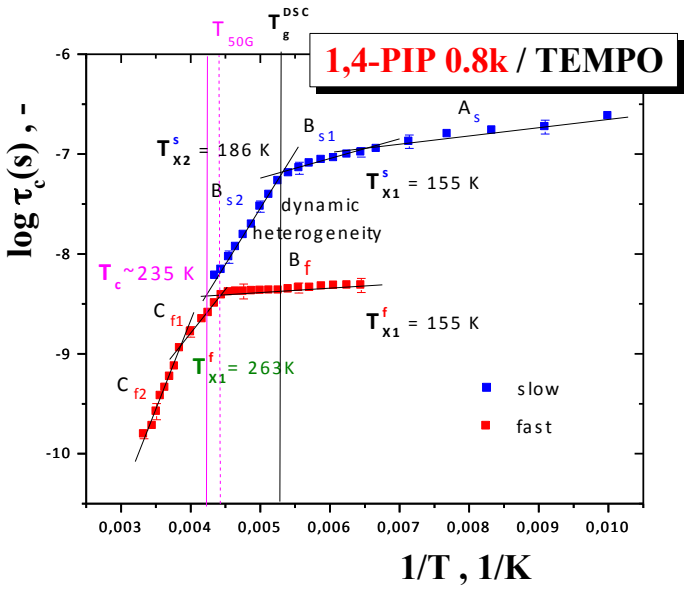

Fig. 4 Arrhenius plot of the correlation time of spin probe **TEMPO** in one - component **1,4-PIP 0.8k** medium indicating the existence of the two low T (A) and high T monomodal regions (C) and the bimodal superimposed region B with the dynamic heterogeneity in the spin probe **TEMPO** mobility.

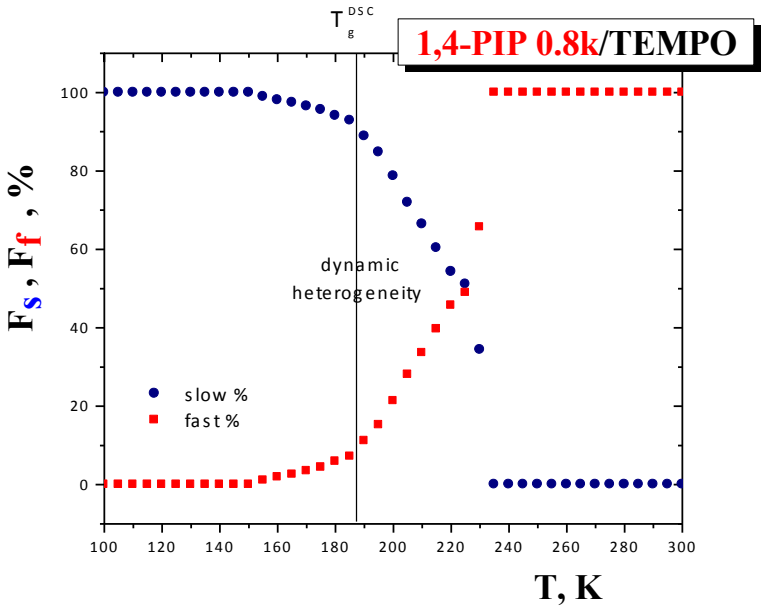

Fig. 5 Fractions of the slow and fast reorienting spin probes **TEMPO** in **1,4-PIP 0.8k** as a function of temperature. The changes in the fraction $F_s = 1 - F_f$ follow those at the characteristic **ESR** temperatures for correlation time in **Fig. 4.**

Three basic motional regions A – C can be distinguished in the Arrhenius plot in **Fig. 4**. In the lowest temperature region A_s from 100 K up to 155 K the **ESR** spectra can be simulated with a single broad triplet from the slowly moving spin probes **TEMPO.** Next, the **ESR** spectra in three subregions of B in between 155 K up to 235 K which consist of two slow regions $\mathbf{B_{s1}}$ (150 K – 180 K) and $\mathbf{B_{s2}}$ from 190 K up to 230 K and one fast zone B_f from 155 K up to 230 K can be simulated by two types of broad and one type of narrow components from the slow and fast spin probes **TEMPO** moving simultaneously. Finally, region C has two sub-regions one C_{f1} from 240 K up to 260 K and another C_{f2} from 260 K up to 300 K. All these regions define the characteristic **ESR** temperatures: $T_{X1}^{s,\tau} = T_{X1}^{f,\tau} = 155$ K, $T_{X2}^{s,\tau} = 186$ K, $T_c \cong 235$ K and finally, $T_{X1}^{f,\tau} = 263$ K. In the further text, the symbol τ_c in the upper index was omitted. The temperature dependence of the fractions of the individual spectral components, F^s, F^f, are given in **Fig. 5**. In general, they exhibit the changes at the characteristic ESR temperatures consistent with the ones in the correlation times.

All the six regions can be described by the Arrhenius equation: $\tau_{c,i}(T) = \tau_{\infty,i} \exp[E_i^*/RT]$ with the pre-exponential factors, $\tau_{\infty,i}$, and activation energies, E_i^*, listed in **Table I**.

Region	**ΔT**, K	$\tau_{\infty,i}$, s	E_i^*, kJ/mol	**r**
A_{slow}	100 – 150	$(3.02\pm0.34)\times10^{-8}$	1.73±0.17	0.953
$B_{slow,1}$	160 – 180	$(1.07\pm0.1)\times10^{-8}$	2.94±0.27	0.976
$B_{slow,2}$	190 – 225	$(2.04\pm0.3)\times10^{-13}$	19.6 ±0.5	0.994
B_{fast}	155 – 220	$(2.69\pm0.06)\times10^{-9}$	0.8 ± 0.04	0.981
$C_{fast,1}$	230 – 255	$(5.25+/-1.7)\times10^{-13}$	16.62+/-0.67	0.993
$C_{fast,2}$	265 – 300	$(4.68+/-0.9)10^{-16}$	31.5+/-2.1	0.974

In a partial summary of this **ESR** part, from a mutual comparison of the respective $\mathbf{2}A_{zz}$, vs. T and log τ_c vs. $1/T$ representations we can see that the later has the larger information content, concerning not only the proportion fraction behavior of the individual spectral components, but especially the superimposed spectral region at intermediate temperaturas. Both the measures of the spin probe mobility provide well comparable pairs of the characteristic **ESR** temperatures with two exceptions. One concerns the start of the fast motion regime which when determined by simulation occurs at essentially lower temperature of 155 K in comparison to that estimated from $\mathbf{2}A_{zz}$, vs. T plot visible at ca. 220 K only. And the second one deals with the main characteristic ESR temperatures T_c and T_{50G}**.** Although these characteristic ESR temperatures are quite close to each other, the former appears at a bit higher temperatures than the latter implying that at T_{50G} some contribution from the slow component still does exist. The relationships between the characteristic ESR temperatures are as follows: $T_{X1}^{s,2Azz'} = 160$ K ≅ $T_{X1}^{s} = T_i^{f} = 155$ K; $T_{X2}^{s,2Azz'} = 190$ K ≅ $T_{X2}^{s} = 186$ K; $T_{50G} = 227$ K ; $T_c \cong 235$ K and $T_{X1}^{f,2Azz'} = 266$ K ≅ $T_{X1}^{f} = 263$ K.

4. Discussion

4.1 The mutual relationships between the ESR and PALS responses

To interpret the physical factors and processes behind a variety of the characteristic **ESR** temperatures, first, the $2A_{zz}$' vs. T and log τ_c vs. $1/T$ dependencies are confronted with the macroscopic **DSC** technique followed by comparison with the microscopic **PALS** one using atomic-sized **o-Ps** probe. In the next chapter, we offer an explanation of some bend effects in the **ESR** and **PALS** response in terms of the features of the relaxation dynamics as obtained by means of **BDS** technique.

In the former molecular and atomic-micro-vs. macroscopic case, the glass-liquid temperature, T_g^{DSC}, is marked as a vertical line in **Figs. 2, 4**, **5** as well as **6** [31]. Good coincidencies exist between T_g^{DSC} and the characteristic **ESR** temperature $T_{X2}^{s,2Azz'} = T_{X2}^{s}$ as well as the characteristic **PALS** one T_g^{PALS} which indicate that all the four phenomena, i.e., an acceleration is the slow regime of **TEMPO** mobility in **Figs. 2** and **4** together with a change in the fraction of the slow and fast components in the superposed spectral region B in **Fig. 5** and the pronounced change in expansion of the **o-Ps** lifetime and related free volume (**Fig. 6**) are very closely interrelated with the thermodynamic glass to liquid transition via the specific heat step variation. It is of interest that the kinetics but not the population of the slow moving spin probes in contrast to the fast reorienting ones is sensitive to this macroscopic transition.

For the latter molecular vs. atomic microscopic case, a comparison at $2A_{zz}$' vs. τ_3 and σ_3 - T level and log τ_c vs. $\tau_3 - 1/T$ one can be made as demonstrated in **Fig. 6** or **Fig. 7.** In both the cases, a number of coincidences can be observed. Thus, the first acceleration in the spin probe **TEMPO** dynamics at $T_{X1}^{s,2Azz'}$ which is consistent with T_{X1}^{s} as well as with T_i^f is not directly related to a change in the **o-Ps** lifetime,τ_3, but rather to that of the **o-Ps** lifetime width, σ_3, at $T_{b1}^{\sigma^3}$ = 162 K due to some very local motion [31]. It is of interest that the onset of the fast motion in the glassy state at T_i^f also correlates nicely with this change in the latter **o-Ps** parameter σ_3. On increase the temperature, the second acceleration in the **TEMPO** reorientation at $T_{X2}^{s,2Azz'}$ = 190 K ≅ T_{X2}^{s} = 186 K coincides with the glass-liquid transition as seen by the PALS technique at T_g^{PALS}. These coincidencies indicate the selective sensitivity of the slow regime but no the fast one of the molecular probe **TEMPO** and the annihilation of

the atomic **o-Ps** one to large-scale segmental dynamics related to T_g^{DSC}. Next, the most pronounced effects in the spin probe **TEMPO** dynamics at $T_c \approx T_{50G}$ lie in the vicinity of the strong bend effect in the PALS response in the liquid state at T_{b1}^{L}**.** This means that the main slow to fast transition in the molecular probe mobility is connected with the strong change in the **o-Ps** lifetime with temperature and the related changed expansion of free volume. In addition, an interesting feature of **Fig. 7** is that the mean time scale of spin probe **TEMPO** reorientation at T_c is comparable to that of **o-Ps** annihilation both reaching a few nanoseconds $\tau_c(T_c) \cong \tau_3(T_{b1}^{L}) \sim 2.1$ ns, the former quantity being in accord with the literature [12]. Finally, in both the plots we observe a closeness between the change in the high T regime of the molecular probe **TEMPO** at T_{X1}^{f} and the **o-Ps** annihilation at T_{b2}^{L}. This suggests on an apparent coincidence between an acceleration of the **TEMPO** within the fast regime and an onset effect in the PALS response for the **o-Ps** probe. However, in contrast to the previous case, we do not observe the *mean* time scale coincidence because of the non-equality:$\tau_c(T_{X1}^{f}) < \tau_3(T_{X2}^{L})$**.** Moreover, it is well known, that the first effect is a true one due to the classic character of the molecular-sized probe which correctly reflects the structural-dynamic change in the medium, while the other one is an artefact of the mutual interaction between the quantum-mechanical **o–Ps** particle and the low viscosity medium [39].

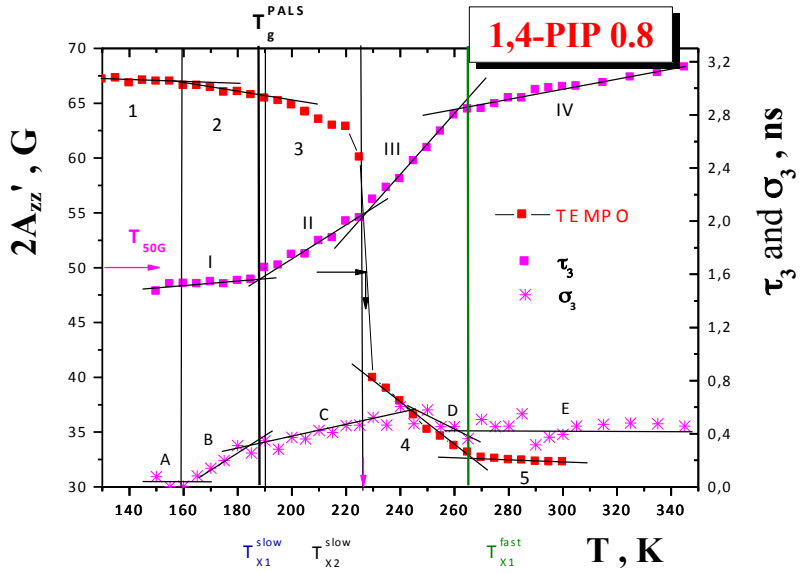

Fig.6 Comparison of the **ESR** response in a form $2A_{zz}$' vs. T with that of **PALS** for **1,4-PIP 0.8k**.

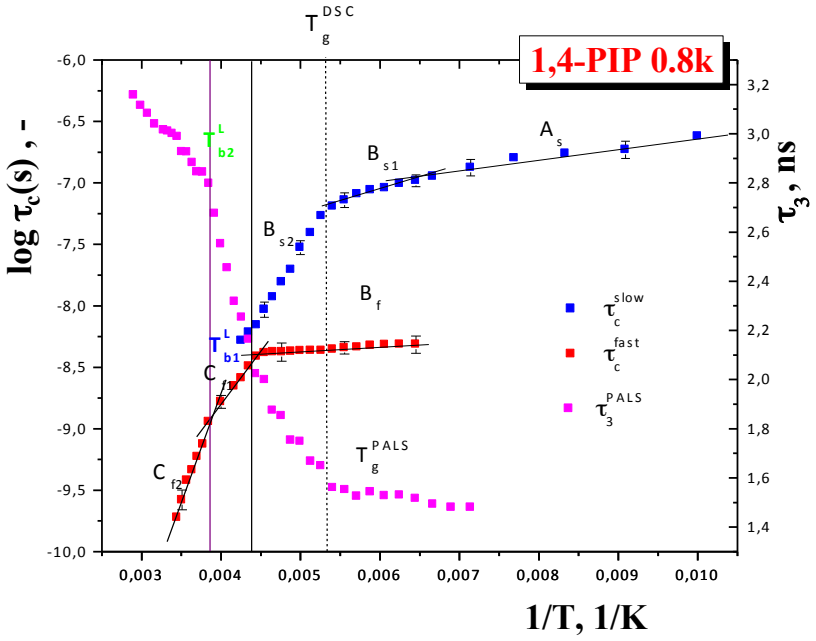

Fig.7 Comparison of the **ESR** and **PALS** time scales in the Arrhenius coordinates: log τ_c vs. $1/T$ and log τ_3 vs. $1/T$ for **1,4-PIP 0.8k.**

4.2 The dynamic origin of the liquid state effects in both the ESR and PALS responses

In the previous paragraph we have presented a series of coincidencies between the characteristic **ESR** and **PALS** temperatures in both the glassy and liquid state as well as between the time scales of the main slow to fast transition of the spin probe **TEMPO** and the **o-Ps** annihilation: $\tau_c(T_c) \cong \tau_3(T_c)$ in **1,4-PIP 0.8k.** These important findings indicate close connections of the both the rotation dynamic and the annihilation phenomena of both the *external* probes and suggest on their common origin which will be addressed in this paragraph.

According to the classic Stockmayer‘s classification of dielectric properties of chain molecules, two basic **Types A** and **B** dipole moments and related dynamic behaviour can be distinguished [40]. Thus, **Type A** chains are characterized by the existence of dipole moment

parallel (*along*) the chain contour causing the low-frequency peak ascribed to the global chain relaxation, while **Type B** chains have dipole moment *perpendicular* (*across*) to the chain backbone reorientation of which causes the high-frequency peak which is attributed to the primary α relaxation due to the cooperative local segmental motion. In the literature, homo-polymeric **cis-1,4-PIP** [41-47] is usually mentioned as typical examples of **Type A** polymers, although it is on the basis of asymmetry of its basic structural unit due to the presence of both the *parallel* and *perpendicular* components of dipole moment evident that cis-**1,4-PIP** belongs rather to a combined **Type A + B** chain systems. **Figs. 8a,b** display dielectric losses of **1,4-PIP 0.8k** over a wide temperature interval from 185 K up to 265 K over a wide frequency range from 10^{-2} up to 10^{9} Hz, i.e., inclusive a high-frequency range relevant for comparison with **ESR** and **PALS** data. Two peak character of the **BDS** spectra in the *liquid* state of **1,4-PIP 0.8k** is confirmed. At low temperatures both the peak features are very strongly overlapped, but on increase of the temperature they become more separated. Consequently, the low frequency peak is attributed to the so-called normal mode relaxation process due to the end-to-end vector reorientation of the whole chain, i.e., a large-scale motion [41f,48], while the higher frequency one stems from the primary α process caused by smaller scale the segmental relaxation of the oligomer and polymer chains [41-47]. The corresponding time scales of both the relaxation processes in **1,4-PIP 0.8k** have been obtained using two phenomenological **Havriliak - Negami (HN)** functions **Eq. 1** in accord with several previous works [42,43]. The maximum relaxation times has been calculated by means of **Eq. 2** and they are plotted in **Fig. 9.** The obtained relaxation times for normal mode, τ_n, being longer than that for the segmental one, τ_α, over the whole measured range from 200 K up to 265 K can be parametrized by the empirical **Vogel-Fulcher-Tamman-Hesse (VFTH)** equations: $\tau_n = \tau_{n\infty} \exp[B/(T-T_{0n})] = 3.2\times10^{-}12\exp[1\ 758.5/(T-136.4)]$ with r = 0.998 and $\tau_\alpha = \tau_{\alpha\infty} \exp[B/(T-T_{0\alpha})] = 2.5\times10^{-14}\exp[1\ 648.7/(T-141.2)]$ with r = 0.996. Now, the time scales of all the three techniques can be compared to identify the dynamic process(es) responsible for the corresponding effects in the **ESR** and **PALS** response.

Fig. 10 displays the two BDS spectra at two selected temperatures in the *liquid* state of **1,4-PIP 0.8k** corresponding to the characteristic **ESR** and **PALS** ones. Thus, the first at $T_c \cong T_{b1}^{L} = 235$ K, where slow to fast transition of the spin probe **TEMPO** in **1,4-PIP 0.8k** occurs coinciding with a change of the slope of **o-Ps** lifetime in the **1,4-PIP 0.8k** medium. For comparison, vertical lines represent the equivalent **ESR** and **PALS** frequencies $f_{c,eq} = 1/(2\pi\tau_c)$ [12b] or $f_{3,eq} = 1/(2\pi\tau_3)$ [20a], respectively. At this temperature the *mean* **ESR** and **PALS** time

scales are equal $\tau_c(T_c) = \tau_3(T_{b1}^L)$ but they are about two orders of magnitude shorter as that of the segmental relaxation $\tau_{\alpha,max}$ ($T_c \cong T_{b1}^L$). On the other hand, they fall into the high-frequency tail of the segmental process indicating that the rapid proportion (fraction) of the primary α process may control the spin probe reorientation **TEMPO** and the expansion of local free volume in the **1,4-PIP 0.8k** medium.

At the second selected temperature close to the characteristic **ESR** temperature, T_{X1}^f, of the first acceleration in the fast regime being comparable with the characteristic **PALS** one, T_{b2}^L, the time scale of the spin probe **TEMPO** rotation is shorter about a factor of 2 than that of the **o-Ps** annihilation: $\tau_c(T_{X1}^f) < \tau_3(T_{b2}^L)$. On the other hand, the PALS time scale is quite close to the maximum of segmental peak in the deconvoluted BDS spectra as often observed in other organic small molecular and polymer glass-formers [14,20-24]. Closer inspection of **Fig. 10** as well as the higher value of the so-called equivalent α temperature defined as $T_\alpha[\tau_\alpha = \tau(T_{b2}^L)]$ = 283 K about of 20 K seems suggest that some further motion could contribute to the plateau effect in the PALS response. Indeed, in **Fig. 10** we can see that also the high-frequency tail of the normal mode reaches the equivalence frequency $f_{3,eq}(T_{b2}^L)$, so that also this larger scale motion could accelerate the onset of the plateau effect. Note that this finding of simultaneous action of both the normal and segmental type of motion seems to be consistent with the small value of the gyration radius $(R^2)^{1/2}$ = 24 Å of oligomeric **1,4-PIP 0.8k** consisting of 12 monomer units only being comparable with the spin probe size of D^W_{TEMPO} = 6.9 Å and suggesting some sensitivity also to the normal mode.

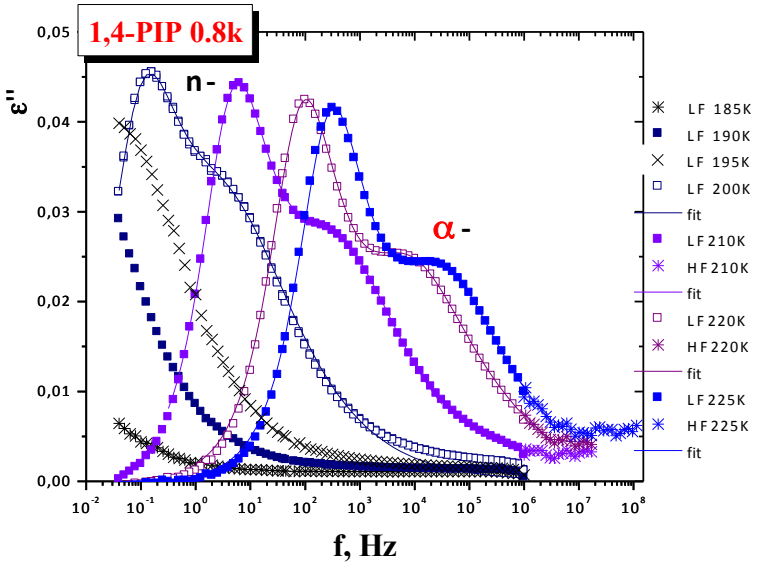

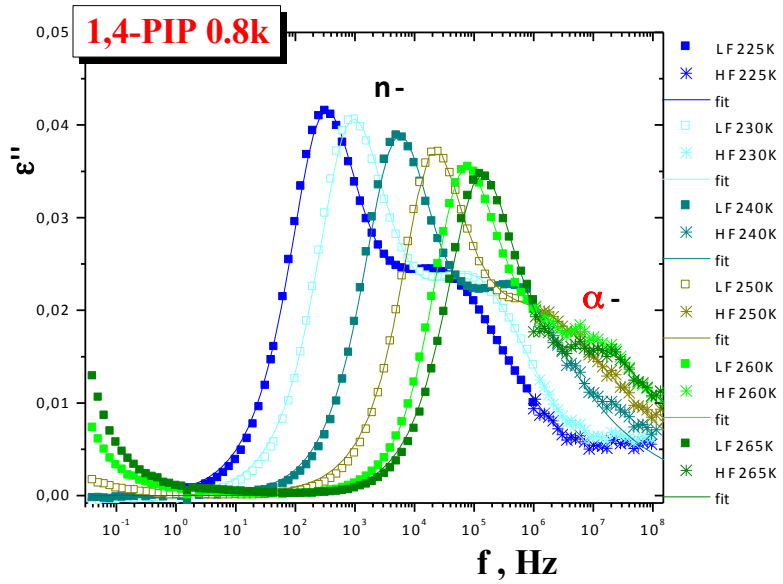

Fig. 8 Dielectric loss of **1,4-PIP 0.8k** as a function of frequency for the temperature range between the coinciding characteristic **ESR** and **PALS** temperatures: **a.** $T_{X2}^{s} \cong T_g^{PALS}$ and $T_c \cong T_{b1}^{L}$ and **b.** $T_c \cong T_{b1}^{L}$ and $T_{X1}^{f} \cong T_{b2}^{L}$ together with the corresponding fitts using two HN functions for the normal mode process and the segmental relaxation.

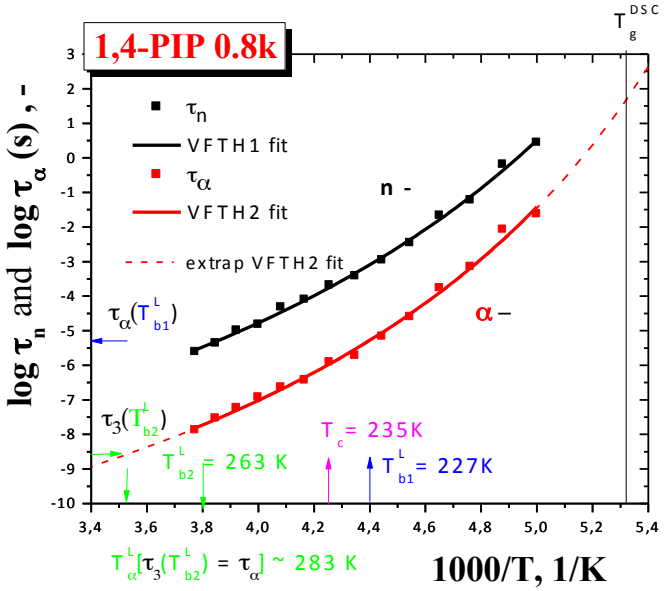

Fig. 9 Relaxation map of **1,4-PIP 0.8k** in the *liquid* state over a range from 200 K up to 265 K with the normal relaxation time, τ_n , and the segmental relaxation times, τ_α , as obtained from phenomenological fittings of the BDS spectra using two overlapping HN functions. The corresponding VFTH equations over a temperature range from 200 K up to 265 K are plotted and the parameters mentioned in the text.To compare the PALS time scale at T_{b2}^{L} with the dielectric relaxation one a slight extrapolation of the VFTH curve over one order of magnitude towards the lower values of the segmental relaxation time is given.

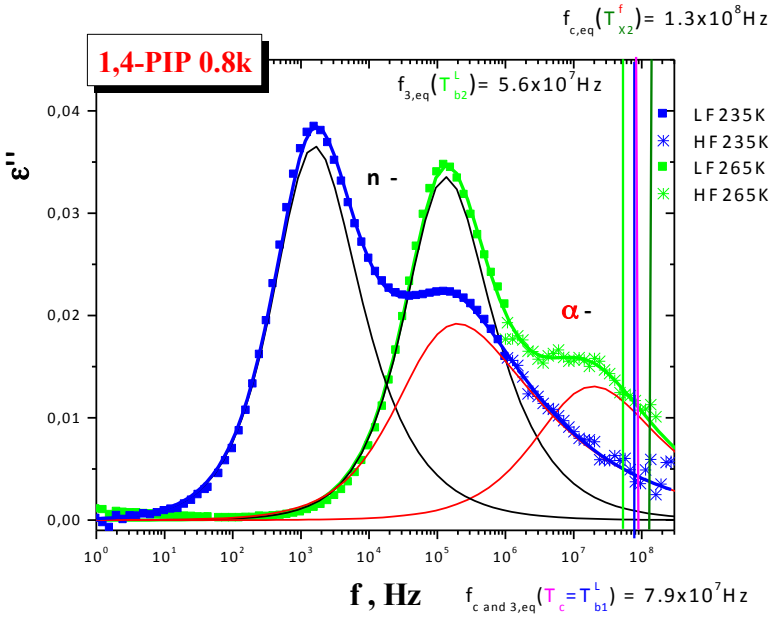

Fig. 10 The BDS spectra at the characteristic ESR and PALS temperatures T_c = 235 K ≅ T_{b1}^{L} with $\tau_c(T_c) = \tau_3(T_{b1}^{L}) < \tau_{\alpha,max}(T_c \cong T_{b1}^{L})$ and $T_{X1}^{f} \cong T_{b2}^{L}$ but with $\tau_c(T_{X1}^{f}) < \tau_3(T_{b2}^{L}) = \tau_{\alpha,max}(T_{X1}^{f} \cong T_{b2}^{L})$. Vertical lines represent the ESR and PALS equivalent frequencies $f_{c,eq} = 1/(2\pi\tau_c)$ or $f_{3,eq} = 1/(2\pi\tau_3)$, respectively.

Conclusions

In summary, the reorientation dynamics of the *molecular*-sized spin probe **TEMPO** in **1,4-PIP 0.8k** together with the annihilation behaviour of the *atomic*-size **o-Ps** probe in **1,4-PIP 0.8k** have been carried out by a joint **ESR** or **PALS** studies, respectively. The changes in the spin probe dynamics are very closely related to the changes in the free volume indicating the common underlying process. This was identified by **BDS** on **1,4-PIP 0.8k** which revealed the presence of the normal-mode and segmental relaxation mode process in the *liquid* state. The spectral simualtions have shown the dynamic heterogeneity of the spin probe **TEMPO** mobility spreaded over 70 K starting in the glassy state at the characteristic ESR and PALS temperatures $T_{X1}^{s} = T_i^{f}$ = 155 K ≅ $T_{b1}{}^{3}$ and ending at the closely coinciding characteristic

ESR and **PALS** temperaures $T_c \cong T_{b1}^{L}$**.** The main finding is that the characteristic **ESR** and **PALS** temperatures in the *liquid* state of **1,4-PIP 0.8k** are in an acceptable agreement suggesting the same origin of the underlying processes, i.e., $T_c \approx T_{50G} \cong T_{b1}^{L}$ and $T_{X2}^{f} \cong T_{X2}^{2Azz'} \cong T_{b2}^{L}$ and that they can be related to the high-frequency tail of the segmental α relaxation peak or the maximum of segmental α relaxation peak, respectively.

Acknowledgments

This work was supported by the European Soft Matter Infrastructure (ESMI) 2011-2012 and 2013 FP7 of EU under Grants No. E111100143 (J.B.) and No. E130100330 (J.B.) as well as by the VEGA Agency, Slovakia under Grant 2/0017/12 (J.B.). We thank Prof.D.E.Budil for providing us with the NLSL program.

References – they will be actualized according to the chosen journal

[1] a. C.A.Angell, Science **267**, 1924 (1995);
b. Ediger MD, Angell CA, Nagel S R. J Phys Chem 1996; B 100, 13200;
c. Angell CA, Ngai KL, Mckenna GB, McMillan PF, Martin SW. J Appl Phys 2000, 88:3113;
d. P. G. Debenedetti and F. H. Stillinger, Nature (London) **410**, 259 (2001).

[2] a. **Growing Length Scales and Their Relation to Timescales in Glass-Forming Liquids**, S. Karmakar, Ch.Dasgupta, S. Sastry, S. Karmakar, Ch. Dasgupta, and S. Sastry Annu. Rev. Condens.Matter Phys. 2014. 5:255;
b.**Glass Transition Thermodynamics and Kinetics,** F. H. Stillinger and P. G. Debenedetti Annu. Rev. Condens. Matter Phys. 2013. 4:6.1;
c. **Perspective: The glass transition** G. Biroli and J. P. Garrahan: J. Chem. Phys. 138, 12A301 (2013);
d. **Perspective: Supercooled liquids and glasses** M. D. Ediger and P. Harrowell J. Chem. Phys. **137**, 080901(2012);
e. **Bond orientational order in liquids: Towards a unified description of water-like anomalies, liquid-liquid transition, glass transition, and crystallization** H. Tanaka Eur. Phys. J. E (2012) **35**: 113;
f. **Theoretical perspective on the glass transition and amorphous materials** L. Berthier, G. Biroli Reviews of Modern Physics 2011,83, 587.

[3] a. S.W.Lovesay et al. *Theory of neutron scattering from condensed matter*, Clarendon Press, Oxford, 1987;
b. M.Beé, *Quasi-elastic neutron scattering*, Adam Hilger, Bristol 1988;
c. Eckstein E, Qian J, Hentschke R, Thurn-Albert T, Steffen W, Fischer EW. J Chem Phys 2000; 113:4751

[4] **Field-cycling NMR relaxometry of viscous liquids and polymers** D. Kruk 1, A. Herrmann, E.A. Rössler Progress in Nuclear Magnetic Resonance Spectroscopy 63 (2012) 33.

[5] a. F.Kremer, A. Schönhals, *Broadband Dielectric Spectroscopy*, Springer, Berlin, 2003;
b. P. Lunkenheimer, M. Köhler, S. Kastner, and A. Loidl in *Structural Glasses and Supercooled Liquids: Theory, Experiment, and Applications*, edited by P. G. Wolynes and V. Lubchenko (Wiley, Hoboken 2012);
c. Alegría A, Goitiandía L, Tellería I, Colmenero J. Recent Res Dev Macromol Res 1998;3: 49.

[6] a. Ngai, KL *Relaxation and Diffusion in Complex Systems*, Springer 2011;
b. Beiner M, Hunt H, Schröter K. J Non-Cryst Solids 2001; 279:126;
c. Ngai KL. J Non-Cryst Solids 2000; 275:7;
d. Sokolov AP.Endeavour 1997; 21:109.

[7] a. Barlow AJ, Lamb J, Matheson AJ. Proc. R. Soc. A 1966; 292:322;
b. Schönhals A, Kremer F, Hofmann A, Fischer EW, Schlösser E. Phys. Rev. Lett. 1993;70: 3459;

c. Stickel F, Fischer EW, Richert RJ. Chem. Phys.1996;104: 2043;
d. Schönhals A. Europhys. Lett. 2001; 56: 815;
e. Alegría A, Colmenero J, Mari PO, Campbell I.A. Phys. Rev. 1999; E 59:6888.
[8] U.Tracht, M.Wilhelm, A.Heuer, H.Feng, K.Schmidt-Rohr, and H.W.Spiess, Phys.Rev.Letts.1998, 81, 2727.
[9] a. **Heterogeneity at the glass transition: a review** Silescu H. J. Non-Cryst. Solids 2000; 243:81;
b. **Spatially heterogeneous dynamics in supercooled liquids** Ediger MD. Ann. Rev. Phys. Chem. 2000; 51:99;
c. **Spatially heterogeneous dynamics in liquids: insights from Simulation** Sharon C. Glotzer, Journal of Non-Crystalline Solids 274 (2000) 342.
d. **Heterogeneous dynamics in liquids: fluctuations in space and time** Richert R. J Phys- Cond.Matter 2002 14 R703.
[10] *Dynamical Heterogeneities in Glasses, Colloids and Granular Materials*, Eds. L. Berthier, G. Biroli, J.-P. Bouchaud, L. Cipelletti, and W. van Saarloos,Oxford University Press, 2011.
[11] a.Dlubek G, *Encyklopedia of Polymer Science and Technology*, in: A.Siedel (Ed.), Wiley & Sons: Hoboken, 2008;
b.*Principles and Application of Positron and Positronium Chemistry*, Y. C. Jean, P. E. Malton, D. S. Schrader, Eds., World Scientific: Singapore 2003;
c.Bartoš J, in *Encyklopedia of Analytical Chemistry*, Meyers, R. A. Eds., Wiley, Chichester, 2000; p 7968
[12] a. *Spin Labelling Theory and Applications*; Berliner, L. J., Ed.; Academic Press: New York, 1978; Vol. 1;
b. Törmälä P., J. Macromol Sci-Rev Macromol Chem 1979; C17:297;
c. Cameron GG. *Comprehensive Polymer Science*, in: C. Booth, C. Price (Eds.), Pergamon Press: Oxford, 1989; vol.1, p.517;
d.Veksli Z, Andreis M., Rakvin B. Prog Polym Sci 2000; 25:949;
e. Andreozzi L, Faetti M, Giordano M, Recent Res. Dev. Phys. Chem 5 (2001) 2895.
[13] a. See e.g. J.John, D.Klepac, M.Didovic, C.J.Sandesh, Y.Liu, V.S.N.Raju, A.Pius, S.Valic, S.Thomas Polymer 51 (2010) 2390.
b. D. Banerjee, S.V. Bhat, D. Leporini, Adv. Chem. Phys. 152 (2013) 1.
[14] a. Tao S, J. Chem. Phys. 56 (1972) 5499;
b. Eldrup M, Lightbody D, Sherwood JN. , Chem.Phys.63 (1981) 51;
c. Nakanishi H, Jean YC, Wang SJ in: S.C. Sharma (Ed.), *Positron Annihilation Studies of Fluids*, World Scientific, Singapore, 1988, p. 292.
[15] Bartoš J, Šauša O, Bandžuch P, Zrubcova J, Krištiak J. J Non-Cryst Solids 2002; 307-310:417-425.
[16] Kilburn D, Wawryszczuk J, Dlubek G, Pionteck J, Hässler R, Alam M A. Macromol Chem Phys 2006; 207:721-34.
[17] G.Dlubek, M.Q.Shaikh, K.Raetzke, M.Paluch, F.Faupel J.Phys.-Cond.Matter **22** (2010) 235104.
[18] Salgueiro W, Somoza A, Silva L, Consolati G, Quasso F, Mansilla M A, Marzocca A, Phys Rev E 2011; 83: 051805-051813.
[19] Pethrick R A, Jacobsen FM, Mogensen OE, Eldrup M. J Chem Soc Faraday Trans 2 1980; 76:225-32
[20] Stevens JR, Chung SH, Horoyski P, Jeffrey KR. J. Non-Cryst. Solids 1994; 172-174: 1207-14.
[21] a. J.Bartoš, O.Šauša, D.Račko, J.Krištiak, J.J.Fontanella, J.Non-Cryst. Solids **351** (2005) 2599;
b. J.Bartoš, O.Šauša, J Krištiak, T Blochowicz, E Rössler, J.Phys. - Condens. Matter **13** (2001) 11473
[22] J.Bartoš, O.Šauša, J.Krištiak, Advanced Research Workshop (ARW) NATO Series: *Nonlinear Dielectric Phenomena in Complex Liquids*, Kluwer Acad. Publ., Dordrecht, The Netherlands, 2004. 289.
[23] J.Bartoš, V.Majernik, M.Iskrova, O.Šauša, J.Krištiak, P.Lunkenheimer, A.Loidl, J.Non-Cryst. Solids **356** (2010) 794.
[24] a. J.Bartoš, G.A.Schwartz, O.Šauša, A.Alegria, J.Krištiak, J.Colmenero, J.Non-Cryst.Solids **356** (2010) 782;
b. J.Bartoš, O.Šauša, G.A.Schwartz, A.Alegria, J.M.Alberdi, J.Krištiak, J.Colmenero, J.Chem.Phys. **134** (2011) 164507;
c. J.Bartoš, O.Šauša, D.Cangialosi, A.Alegria, H. Švajdlenkova, J.Krištiak, A.Arbe, J.Colmenero, J.Phys.-Cond. Matter **24** (2012) 155104;
d.Y.Yu, G.Dlubek, J.Bartoš, H.Švajdlenková, R.Krause-Rehberg, Mat. Sci.Forum.
[25] J.Bartoš, O.Šauša, M.Köhler, H.Švajdlenková, P.Lunkenheimer, J.Krištiak, A. Loidl, J.Non-Cryst.Solids **357** (2011) 376.
[26] G.P.Rabold, J.Polym.Sci. A17 (1969) 121.
[27] H.Švajdlenková, J.Bartoš, J.Polym.Sci. B Polym.Phys. **47** (2009) 1058.
[28] H.Švajdlenková, O.Šauša, M.Iskrová-Miklošovičová, V.Majerník, J.Krištiak, J.Bartoš, Chem.Phys.Lett. **539–540** (2012) 39.
[29] H.Švajdlenková, M.Iskrová, O.Šauša, G.Dlubek, J.Krištiak, J.Bartoš, Macromol. Symp. **305** (2011)108.
[30] J.Bartoš, H.Švajdlenková, Y.Yu, G.Dlubek, R.Krause-Rehberg, Chem.Phys.Letts. **584** (2013) 88.

[31] J.Bartoš, H.Švajdlenková, M.Lukešová,Y.Yu, R.Krause-Rehberg, Chem.Phys.Letts. **602** (2014) 28.
[32] S. Hwang, R.P. Mason, L.P. Hwang, J.H. Freed, J. Phys. Chem. 79 (1974) 489.
[33] D.E. Budil, S. Lee, S. Saxena, J.H. Freed, J. Magn. Reson. A120 (1996) 155.
[34] S.V. Paschenko, Yu.V. Toropov, S.A. Dzuba, Yu.D. Tsvetkov, V.Kh. Vorobiev, J. Chem. Phys. 110 (1999) 8150.
[35] D.A. Chernova, A.Kh. Vorobiev, J. Polym. Sci. B 47 (2009) 107.
[36] S. Havriliak, S.N. Negami, J. Polym. Sci. C **14**, 99 (1966)
[37] a. A. Boersma A, van Turnhout J, Wübbenhorst M. Macromolecules **31** 7453 (1998);
b. K.Schröter, R.Unger, S.Reissig, F.Garwe, S.Kahle, M.Beiner, E.Donth in *Dielectric and Mechanical Relaxation on Materials*, Hanser, Münich, 1997 p.57
c. R.Diaz-Calleja Macromolecules 33, 8924 (2000)
[38] Cameron GG, Stewart D. Eur Polym 1993; 29:245
[39] Winberg P, Eldrup M and Maurer F H J 2012 *J Chem Phys* **136** 244902
[40] W.H. Stockmayer Pure Appl. Chem. **15** 539 (1967)
[41] a. K.Adachi, T.Kotaka Macromolecules 17, 120 (1984)
b. K.Adachi,T.Kotaka Macromolecules 18, 466 (1985)
c. K.Adachi, J. Kotaka J. Mol. Liquids 36, 75 (1987);
d. K.Adachi, T. Kotaka Macromolecules 21, 157 (1988);
e. Y.Imanishi, K.Adachi, T.Kotaka J.Chem.Phys. 89, 7585 and 7593 (1988)
f. K.Adachi, T.Kotaka Progr.Polym. Sci. 18, 585 (1993)
[42] D.Boese, F. Kremer Macromolecules 23, 829 (1990)
[43] A.Schönhals, Macromolecules 28, 1309 (1993)
[44] M.Doxastakis, D.N.Theodorou, G.Fytas, F.Kremer, R.Faller, F.Müller-Plathe, N.Hadjichristidis J.Chem. Phys.119, 6883 (2003)
[45] A.P.Sokolov,Y.Hayashi J. Non - Cryst. Solids 353, 3838 (2007)
[46] C.Riedel, A. Alegria, P.Tordjemna, J.Colmenero Macromolecules 42, 8492 (2009)
[47] A.Abou Elfadl, R.Kahlau, A.Herrmann, V. N.Novikov, E.A.Rössler *Macromolecules,* 43, 3340 (2010)
[48]a. P.E.Rouse J. Chem. Phys. 21, 1272 (1953),
b. M. Doi, S.F.Edwards *The theory of polymer dynamics* Clarendon, Oxford, 1986.